Mo Jiang
Richard D. Braatz*

Low-Cost Noninvasive Real-Time Imaging for Tubular Continuous-Flow Crystallization

A key design limitation to the effective monitoring and control of continuous crystallization processes is the ability to characterize crystals in real time. A low-cost system composed of a basic stereomicroscope and video camera for the in situ imaging of sub-millimeter crystals through curved walls of millifluidic tubular crystallizers is described. Real-time videos taken for millimeter-size slurry slugs are used to guide the experimental design for a recently developed multiphase-flow crystallization process, including the improvement of the slug aspect ratio, visualization of crystal shapes, and observation of the extent of aggregation. Design considerations are also discussed for the use of multiple stereomicroscopes in other continuous-flow tubular experiments.

Keywords: Continuous crystallization, Imaging technology, Inline monitoring, Multiphase flow, Tubular crystallizer

Received: May 07, 2016; *revised:* May 02, 2017; *accepted:* September 15, 2017

DOI: 10.1002/ceat.201600276

Supporting Information available online

1 Introduction

Continuous crystallization has received increasing attention in pharmaceutical manufacturing due to its high process efficiency and flexibility [1–8]. Millifluidic tubular crystallizers with practical production capacity is of recent interest [7], but obtaining real-time information on the crystals inside such crystallizers has been limited by available techniques. The main focus in the literature for relevant problems has been the development of imaging systems in stirred-tank crystallizers [8–17]. Most of these imaging systems [8–17] use sampling, in situ probes, or flow-through cell imaging devices to directly monitor the dynamic variation of crystal size, shape, and polymorphic form.

Sampling is a helpful and standard experimental approach, but its drawbacks include yield reduction if the sample slurry is pulled out of the system, the increased potential for clogging if the sampling system is connected to the main crystallizer, and that the collected crystals may not be representative of the slurry. Commercial in situ imaging probes can provide real-time crystal images with the probes inserted in the crystallizer (the working distance is less than the crystallizer wall thickness), at a high capital cost, typically $100 000 or more such as the particle vision measurement (PVM) [18–22]. The measured crystals may not be representative of the slurry as well, and the introduction of new surfaces, e.g., of probe tips, to the crystallizer can also lead to increasing fouling. Flow-through cell imaging devices through a flat transparent surface built into the crystallizer wall [8, 18, 23] allow substantial improvement of image quality and the size of imaging plane at a reduced cost. But similar to an inline sample system, the devices have an increased potential for clogging and fouling by introducing new surfaces, i.e., the imaging cell, and by having the slurry flow through changing geometries.

Compared to stirred-tank batch crystallizers [21, 22, 24], much fewer studies have explored imaging techniques for continuous tubular crystallizers or particles in flow due to the intrinsic difficulty of monitoring continuous process [5, 7, 8, 25, 26]. A batch crystallizer may only require one imaging probe/sensor to monitor all of its transient operation, but obtaining similar information in the corresponding continuous process requires measurement at multiple spatial locations along the tube. As such, the cost and operational problems per probe for a continuous crystallizer must be at least an order of magnitude lower than for stirred tanks. Based on experience from stirred-tank crystallizers, there is a strong preference for the inline imaging of continuous crystallization to be noninvasive, that is, it does not employ sampling of any type and does not introduce any new surfaces that can induce fouling or constrictions to flow that can induce clogging. It is also desired to avoid technical/operational difficulties associated with any fitting of the imaging probe/sensor to the desired crystallizer dimension, and to allow a large size of the imaging plane and depth of field [27] through a crystallizer wall without having to change the local geometries [8, 18, 23, 25].

This paper demonstrates and analyzes an inexpensive imaging system composed of a basic stereomicroscope for both inline monitoring and offline imaging in a recently developed

Dr. Mo Jiang, Prof. Richard D. Braatz
braatz@mit.edu
Massachusetts Institute of Technology, Department of Chemical Engineering, 77 Massachusetts Avenue, 02139, Cambridge, MA, USA.

multiphase-flow continuous crystallizer through the curved tubing wall [7, 28]. Stereomicroscopes are widely used in the biological/medical fields [29] and in jewelry making and watch repair [29] for 3D ("stereo", through viewing from two eyepieces at the same time) visualization of samples/pieces, e.g., during preparation/operation, due to its large working distance and depth of field. While still allowing for 3D "stereo" imaging using stereomicroscope eyepieces by operators during experiments as in applications involving microfluidics [29], here also a stereomicroscope for real-time video imaging of millifluidic flow systems is applied.

The inline videos and offline images use 2D visualizations with the main optical path connected to a camera, which is the same kind of visualization as the compound microscopes commonly taken for crystal imaging [4, 20, 28], but with a larger depth of field and much lower complexity and cost [27]. The large depth of field in a stereomicroscope allows the direct imaging of particles as they move under flow in tubes with transparent walls. With the total cost, of $500, including the stereomicroscope, camera, and acquisition software, being about an order of magnitude less than any other imaging system for similar purposes, this stereomicroscope-based robust tool can be used in a large number along tubular systems. Deep comprehension of inline images of crystallization phenomena in continuous flow are provided, with practical considerations for design and operations of flow systems discussed beyond crystallization.

2 Equipment and Experiments

As illustrated in Fig. 1, the key imaging part is a trinocular stereomicroscope (model #XV331AC20C from Cyber Scientific Corporation, with built-in objectives 1× and 3×, and eyepiece objectives of 10× and 30×) connected to (not through eyepieces) a camera (model #DFK 22BUC03, with 1/3" Micron CMOS MT9V024 sensor and software IC Capture v2.2, from The Imaging Source, LLC), the same as in [28]. The software allows the user to set all camera parameters, to see live image data streams from the camera, to take single images or image sequences from the camera and save as BMP or JPG files, and to capture real-time videos as AVI files for post-processing. Cooling crystallization with slug flow was chosen to demonstrate the imaging system. The solute was the well-studied *L*-asparagine monohydrate (LAM, purity ≥ 99 %, from Sigma-Aldrich) [7, 11, 28] and the solvent was deionized (DI) water. LAM in aqueous solution is an interesting model system due to its ability to form crystals of varying shape and its tendency to aggregate, depending on the crystallizer design and its operating conditions.

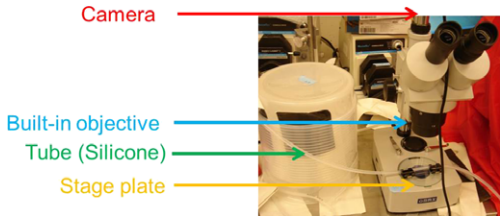

Figure 1. Stereomicroscope-based imaging equipment on the right of figure and tubing where slugs flow on the left of figure. The imaging section (using a camera connected to stereomicroscope, not shown in the figure) of the tubing is between two black channel clamps for securing the position of the tubing during slug flow, on top of the stage plate in the photograph. The transmitted light source is under the stage plate. The focus stroke/knob is on the right side of the stereomicroscope, not shown from this angle of the photograph. All microscope images in this article were taken as normal 2D images, rather than as 3D images.

The process intensification strategy of decoupling nucleation and growth from [7] and [28] was adopted here, and the stereomicroscope was only applied to the growth stage where the total number of crystals remains the same, for the convenience of tracking the same crystal between adjacent screenshots as detailed in the next section. In the nucleation experimental subsystem, a peristaltic pump was used to feed supersaturated LAM solution into a 2 m long Masterflex Biopharm silicone tube with 3.1 mm inner diameter. About 1.3 m of tubing downstream from the feed solution, crystals were nucleated either with mixing hot and cold solutions in coaxial/radial micromixers [7], or with an ultrasonication probe pressed against the tube [28]. About 0.7 m of tubing downstream from the nucleation zone, e.g., coaxial/radial micromixers [7] or an ultrasonication probe [28], the slurry entered one end of a slug-forming T-mixer, with the other entrance being air-fed using a peristaltic pump.

The growth subsystem was composed of a 15.2 m long Pharma-80 silicone tube with an inner diameter of 3.1 mm and an outer diameter of ~ 6 mm that connected to the exit of the slug-forming T-mixer. The air and slurry flow rates were selected as described in [7] and [28] such that alternative slugs of air and slurry spontaneously form at the exit of the T-mixer and remain stable throughout the tube due to the strong surface tension force relative to gravitational and other forces. In the growth zone downstream from the slug-forming T-mixer, the seed crystals from nucleation continued to grow in the slurry slugs as they moved down the tube until manual collection into polystyrene wells in a well plate [28]. The growth of crystals was driven by natural cooling of slurry slugs at ~ 30 °C to room temperature (20 °C) of tubing wall and air slug. Videos of slurry slugs were taken through the silicone tube (Dow Corning Pharma-80) in which slugs flow and offline images were taken inside wells.

3 Results and Discussion

The first part of this section demonstrates the application of the stereomicroscope-based imaging system to optimize the design and operations of a slug-flow tubular crystallizer. Then, more general guidance is provided on the optimal placement and operation of the imaging systems for the real-time spatial monitoring of multiphase flow processes.

3.1 Stereomicroscopes for Insights into Slug-Flow Crystallization Process Design

Fig. 2 demonstrates the feasibility of a stereomicroscope for real-time monitoring of slugs (one dimension is the same as the tubing inner diameter of ~ 3 mm) inside the curved surface of a tubing wall with thickness of ~ 1.5 mm. These screenshots provide a direct view into the system, which facilitates identification of the key physical phenomena that can be used to optimize the operating conditions as discussed in more detail below.

The clear view of slug shape is useful for informing the selection of tubing material and size. The affinity of solvent water to the material of the inner tubing wall is more obvious at the front of a moving slug, rather than the concave back of the slurry slug with respect to flow direction (Fig. 2) due to wall drag on the liquid. The closer the slug shape is to a sphere, the smaller the volume of any dead zone and the better the mixing. When the aqueous slugs are not moving, the front and back of the slugs are flat surfaces for the Pharma-80 silicone tubing, i.e., each slug is a cylinder, compared to a concave shape in hydrophilic tubing materials, e.g., quartz tubing, see Fig. S1, Supporting Information. The Pharma-80 tubing was also chosen for non-stickiness of particles, as shown in video snapshots (Fig. 2), which are also useful to check the effectiveness of any cleaning procedure and locate any positions where additional cleaning is needed. The whole width of the inner tubing can be viewed and imaged within one image frame with reasonable effective resolution for the crystals (Fig. 2). Tubing of a larger diameter has a higher production rate for the same flow velocity, but may also generate more waste, and reduces the operating region in which slugs are stable [7].

The imaging system was used to optimize the aspect ratio of the slurry slugs based on visualizing the motion of the crystals within each slug, with the aspect ratio specified by varying the ratio of air to liquid flow rates within the flow regime in which slugs are hydrodynamically stable [7]. The slug aspect ratio of ~ 1 was observed to produce the best mixing (Figs. 2 b) and 2 c. In a slug with a high aspect ratio (Figs. 2 a, 2 b), crystals tend to stay at the back of the slugs with respect to the flow direction, as the crystals had a larger density/inertia than the liquid solution. The higher the proportion of crystals at the back of slugs, the higher the rate of crystal-crystal contacts and the higher the probability of secondary nucleation. Crystals in slugs with an aspect ratio closer to 1 are more spread out in each slug, which is closer to behaving like an ideally mixed batch crystallizer moving down the tube. The visualization system shows that crystals stay close to the center rather than near the wall (Figs. 2 c, 2 d), which is presumably due to the flow that moves particles near the back of the slug to the centerline not having enough drag force on the crystals to push them up the centerline to the front of the slug. The spatial location of most crystals near the centerline implies a low probability that crystals can stick to the tubing walls.

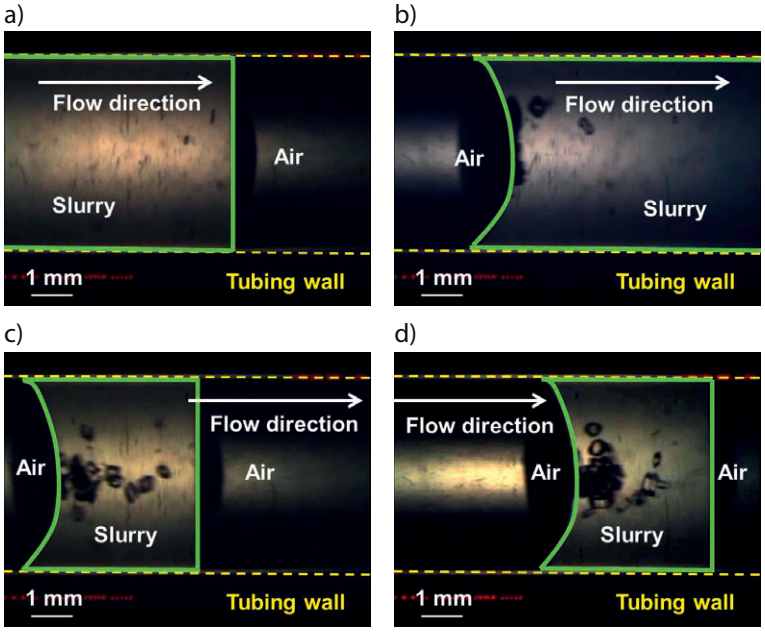

Figure 2. Inline stereomicroscope video snapshots of (a) the front and (b) the end of a slurry slug with an aspect ratio close to 4, and at (c) an earlier time and (d) later time of another slurry slug with an aspect ratio of about 1. Slurry slugs (slug boundaries highlighted in green solid lines/curves, with the same symbols for Figs. 3 and 4) are separated by air slugs inside a silicone tube (two inner walls indicated in yellow dashed lines, with the same symbols for Figs. 3 and 4). The black shade at two air/slurry interfaces is due to curvature. The videos for the snapshots were taken at an exposure time of 1/500 s and a maximum frame rate of 76 fps, with light intensity adjusted for the best possible image with current equipment; (b) and (c) are modified based on [7], with reprint permission granted.

Crystals generated in the solute-solvent system in this study, LAM in aqueous solution, have a high tendency to aggregate, depending on the operating conditions, which is usually undesirable for controlling crystal size distribution. While aggregation can be observed in offline images of the product crystals (Fig. 3 a), it is typically not clear whether crystal aggregates observed at that stage were generated during crystallization, filtration, or drying. Real-time imaging is faster and more reliable for adjusting the experimental conditions to minimize aggregation and material waste, e.g., can stop experiments as soon as any aggregation is observed. The use of a stereomicroscope for the real-time characterization of aggregation is demonstrated in Fig. 3 b. The nucleation conditions used in Figs. 2 c and 2 d were evaluated and improved starting from the preliminary conditions applied in Figs. 3 and 4. In particular, based on Fig. 3 b and similar images, the average solute concentration for cooling crystallization was reduced, which decreased the overall supersaturation at the same temperature and was observed to diminish aggregation (Figs. 2 c, 2 d).

The crystals generated in the solute-solvent system in this study can have different shapes, depending on the experimental conditions. The real-time imaging from a stereomicroscope can facilitate the quick search of experimental conditions towards manufacturing crystals with shapes

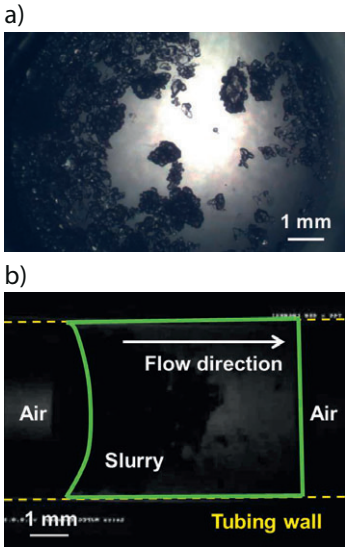

Figure 3. (a) Offline stereomicroscope image of representative slurry slugs in the same experiment as in (b). The image was taken at an exposure time of 1/4 s, with light intensity adjusted to obtain the best image with the equipment. (b) An inline stereomicroscope video snapshots of a slurry slug containing aggregation, e.g., indicated by the irregular black area at the back of the slurry slug. The imaging settings for (b) are the same as in Fig. 2. The experimental conditions are the same as Figs. 2 c and 2 d except that the average solute concentration in this figure is higher and the resulting slug uniformity was lower.

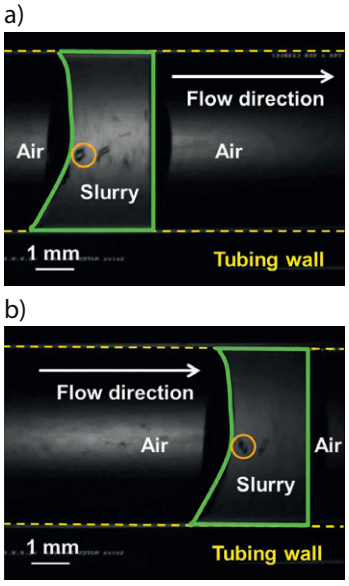

Figure 4. Inline stereomicroscope video snapshots of a slurry slug at (a) an earlier time and (b) later time. The imaging settings are the same as in Fig. 2. Stereomicroscopy helps identify 3D shapes of crystals as they rotate in recirculation, such as the two large crystals in the center left of the slugs in the two images, and distinguish different shapes of crystals such as between Figs. 2 c, d and this figure, without needing to focus two cameras at different angles which requires maintenance of alignment and calculation of shape. The experimental conditions are the same as for Figs. 2 c and 2 d except that the slug aspect ratio is much smaller, the starting configuration used air as its cold inlet stream instead of liquid solution, and the initial solute concentration in the hot stream was lower (0.09 g solute/g solvent).

that are more conducive to downstream processing such as filtration, drying, and tableting. Imaging of the same slug at different times allows an observation of individual crystals rotating in the slug during recirculation, providing an additional angle than using offline images. For example, the crystal nearest the back of a slug in the preliminary experiment in the orange circle in Fig. 4 a is the same crystal as the similarly located crystal near the back of the slug in the orange circle in Fig. 4 b with different 2D projections, showing more information on the crystal shape, compared to offline images. Several rounds of improvement resulted in the experimental conditions used in Figs. 2 c and 2 d, in which the crystals are cube-like as confirmed with offline measurements, with an aspect ratio near 1 that is easier to handle in downstream processing.

The offline images of the product crystals in collection wells (Fig. 5), have enough resolution for collecting particle size statistics [7, 28]. The large imaging plane, e.g., the size of the whole imaging cell that holds slugs as in Fig. 5, can conveniently facilitate estimation of the crystal size uniformity with reasonable accuracy, for a whole sample, e.g., three to four slugs, in each well. For instance, the effectiveness of controlled primary nucleation, e.g., with indirect sonication, followed by nearly pure growth to produce large uniform-sized crystals [28] with low aspect ratio and negligible aggregation is demonstrated in Fig. 5, for this system that has a high tendency towards aggregation [7, 28].

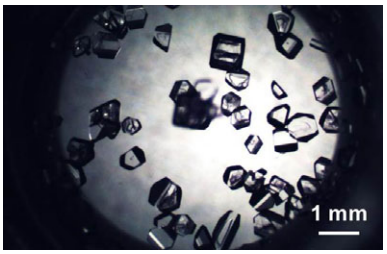

Figure 5. Offline stereomicroscope images of crystals from representative slurry slugs with nuclei generated by indirect sonication followed by growth in slugs; experimental conditions for slug-flow crystallization are the same as in [7, 28]. The dark ring-shape shade on the edges is due to the different refractive index between corn oil (brighter areas) and water. The dark cluster in the center are floating crystals, probably due to surface tension, which can be identified from focusing the imaging plane at the upper and lower surfaces of the collection well (not shown).

3.2 Suggested Design and Operation of Real-Time Imaging in Continuous-Flow Experiments

3.2.1 Setting the Spatial Locations and Total Number of Stereomicroscopes (Sensors)

For imaging in tubular continuous multiphase flow operations, multiple sensors along the length of the tube can be helpful for providing real-time images and data like particle size distribution to evaluate and improve operating conditions such as feed flow rates and starting concentration/temperature. Due to the one-to-one relationship between batch and continuous tubular operations, e.g., the time operating in a batch process corresponds to the residence time in a tubular process, the spatial locations of these sensors can mimic the time profile for the batch process [7, 20]. The total number of stereomicroscopes for continuous-flow processes mimics the total sampling points for batches, but without having to drawing out samples.

As for batches, the total number and time interval for sampling depend on the specific systems and available resources. Possible ways to set up the spatial locations of these sensors is to maintain constant time, or temperature, or solution concentration intervals between adjacent sensors. More sensors should be placed at process stages that require more frequent measurement. The low cost of the stereomicroscopic imaging system allows design and implementation for the users' convenience, e.g., placed at a large number of spatial locations, while being a minimum fraction of the total process cost.

3.2.2 Adjusting Configuration and Operation Parameters of Stereomicroscopes

Transparent tubing was selected, allowing imaging through the tubing wall with the transmission mode of stereomicroscopes. For example, slugs inside Pharma-80 silicone can be imaged even with 1.5 mm thickness of the tubing wall; e.g., Figs. 2 and 4. Glass tubing would be fine for imaging as it is transparent, but glass is easy to break. The selection of tubing material also considered non-stickiness so as to prevent material transfer from one slug to another and to minimize fouling. Other advanced microscopes may have a reflection mode, but those are not the focus of this discussion. For the slug-flow system, the reflection mode did not contribute to high-quality imaging, thus was not used here.

Then, the focal plane was adjusted with the focus stroke, and imaging quality further checked, e.g., crystals, by testing different objectives. In the slug-flow video snapshot examples like in Figs. 2 and 4, the focal plane was at the middle height of tubing, for a consistent plane of image and the largest, or widest, view of the area of interest, also for convenient operation. A stereomicroscope usually does not have high-magnification options that reduce the size of the imaging plane, and a low magnification can be enough for particles of at least a couple of hundred micrometers in size if focused on the right plane; see, e.g., Figs. 2 c and 2 d with 1× magnification from the built-in objective of the stereomicroscope together with its intermediate magnifying lens for process monitoring. The resolution may be improved with similar add-on modules for microfluidics [29]. With a large working distance, i.e., 10.2 cm, according to vendor, for the stereomicroscope, the sample holder has many other options including well plates and vials.

4 Conclusions

An imaging system based on a stereomicroscope is demonstrated for the visualization and design guidance for a slug-flow continuous crystallization process. Based on analysis of the inline and offline images, equipment designs were improved, such as tubing material and dimensions, and experimental conditions were quickly tested and enhanced, such as the ratio of air to water flow rates to generate slugs with better mixing.

While some other crystallization imaging systems also do not require direct contact with the crystal slurry [10, 18], this stereomicroscope imaging system has two unique advantages for multiphase continuous flow: (1) a large working distance on the order of 10 cm, allowing imaging through a curved surface, e.g., a tubing wall of 1.5 mm thickness, with a large imaging plane, e.g., to cover the whole width of millimeter size tubing; and (2) very low cost, feasible to place dozens of systems along a tubular crystallizer at the cost of one other imaging system, with simple implementation/usage/maintenance. This system is a good complement to current offline imaging technology for quick online monitoring, for example, to observe in real time abnormal operations such as undesired aggregation, agglomeration, or crystal shape.

This stereomicroscope imaging system is applicable to other tubular systems that contain dispersed phases, such as crystallization, liquid-liquid dispersions, or flow chemistries that continuously form particles [3]. Also, guidelines are provided for designing stereomicroscope imaging systems for these new continuous-flow experiments, including the number and spatial location of imaging systems and the choice of operating parameters. As any other system, this imaging system has application limits, which can be reduced with hardware upgrades. For example, a basic stereomicroscope does not have polarizers, thus the crystalline form has to be confirmed with a microscope equipped with polarizers, or an advanced stereomicroscope. For more quantitative analysis such as estimating the crystal number and size in real time, the current imaging system can be upgraded with a stronger light source and camera to improve the contrast; note the intrinsic difficulty of non-invasive imaging through a thick curved wall.

Acknowledgment

Novartis Pharmaceuticals is acknowledged for financial support. Dr. Jun Xu is thanked for technical discussion on camera selection.

The authors have declared no conflict of interest.

References

[1] A. S. Myerson, *Handbook of Industrial Crystallization*, 2nd ed., Butterworth-Heinemann, Woburn, MA **2002**.

[2] A. S. Myerson, M. Krumme, M. Nasr, H. Thomas, R. D. Braatz, *J. Pharm. Sci.* **2015**, *104 (3)*, 832–839. DOI: 10.1002/jps.24311

[3] I. R. Baxendale, R. D. Braatz, A. J. Florence, B. K. Hodnett, K. F. Jensen, M. D. Johnson, P. Sharratt, J. Sherlock, *J. Pharm. Sci.* **2015**, *104 (3)*, 781–791. DOI: 10.1002/jps.24252

[4] M. Jiang, Y.-E. Li, H.-H. Tung, R. D. Braatz, *Chem. Eng. Process.* **2015**, *97*, 242–247. DOI: 10.1016/j.cep.2015.09.005

[5] C. J. Brown, X. W. Ni, *Cryst. Growth Des.* **2011**, *11 (9)*, 3994–4000. DOI: 10.1021/cg200560b

[6] Z. K. Nagy, R. D. Braatz, *Annu. Rev. Chem. Biomol. Eng.* **2012**, *3*, 55–75. DOI: 10.1146/annurev-chembioeng-062011-081043

[7] M. Jiang, Z. Zhu, E. Jimenez, C. D. Papageorgiou, J. Waetzig, A. Hardy, M. Langston, R. D. Braatz, *Cryst. Growth Des.* **2014**, *14 (2)*, 851–860. DOI: 10.1021/cg401715e

[8] S. Schorsch, D. R. Ochsenbein, T. Vetter, M. Morari, M. Mazzotti, *Chem. Eng. Sci.* **2014**, *105*, 155–168. DOI: 10.1016/j.ces.2013.11.003

[9] J. Calderon De Anda, X. Z. Wang, X. Lai, K. J. Roberts, *J. Process Control.* **2005**, *15 (7)*, 785–797. DOI: 10.1016/j.jprocont.2005.02.002

[10] P. A. Larsen, J. B. Rawlings, *AIChE J.* **2009**, *55 (4)*, 896–905. DOI: 10.1002/aic.11739

[11] M. Jiang, C. Gu, R. D. Braatz, *Chem. Eng. Process.* **2015**, *97*, 187–194. DOI: 10.1016/j.cep.2015.06.013

[12] R. F. Li, R. Penchev, V. Ramachandran, K. J. Roberts, X. Z. Wang, R. J. Tweedie, A. Prior, J. W. Gerritsen, F. M. Hugen, *Org. Process Res. Dev.* **2008**, *12 (5)*, 837–849. DOI: 10.1021/op800011v

[13] D. B. Patience, J. B. Rawlings, *AIChE J.* **2001**, *47 (9)*, 2125–2130. DOI: 10.1002/aic.690470922

[14] P. A. Larsen, D. B. Patience, J. B. Rawlings, *IEEE Control Syst. Mag.* **2006**, *26 (4)*, 70–80. DOI: 10.1109/MCS.2006.1657878

[15] M. Kempkes, J. Eggers, M. Mazzotti, *Chem. Eng. Sci.* **2008**, *63 (19)*, 4656–4675. DOI: 10.1016/j.ces.2007.10.030

[16] M. Kempkes, E. Darakis, T. Khanam, A. Rajendran, V. Kariwala, M. Mazzotti, T. J. Naughton, A. K. Asundi, *Opt. Express.* **2009**, *17 (4)*, 2938–2943. DOI: 10.1364/OE.17.002938

[17] L. L. Simon, T. Merz, S. Dubuis, A. Lieb, K. Hungerbuhler, *Chem. Eng. Res. Des.* **2012**, *90 (11)*, 1847–1855. DOI: 10.1016/j.cherd.2012.03.023

[18] X. Z. Wang, K. J. Roberts, C. Ma, *Chem. Eng. Sci.* **2008**, *63 (5)*, 1173–1184. DOI: 10.1016/j.ces.2007.07.018

[19] L. L. Simon, Z. K. Nagy, K. Hungerbuhler, *Chem. Eng. Sci.* **2009**, *64 (14)*, 3344–3351. DOI: 10.1016/j.ces.2009.04.016

[20] S. Wang, M. Jiang, S. Ibrahim, J. Wu, X. Feng, X. Duan, C. Yang, N. Ohmura, *Chem. Eng. Technol.* **2016**, *39 (4)*, 680–688. DOI: 10.1002/ceat.201500458

[21] L. L. Simon, H. Pataki, G. Marosi, F. Meemken, K. Hungerbühler, A. Baiker, S. Tummala, B. Glennon, M. Kuentz, G. Steele, H. J. M. Kramer, J. W. Rydzak, Z. Chen, J. Morris, F. Kjell, R. Singh, R. Gani, K. V. Gernaey, M. Louhi-Kultanen, J. O'Reilly, N. Sandler, O. Antikainen, J. Yliruusi, P. Frohberg, J. Ulrich, R. D. Braatz, T. Leyssens, M. von Stosch, R. Oliveira, R. B. H. Tan, H. Wu, M. Khan, D. O'Grady, A. Pandey, R. Westra, E. Delle-Case, D. Pape, D. Angelosante, Y. Maret, O. Steiger, M. Lenner, K. Abbou-Oucherif, Z. K. Nagy, J. D. Litster, V. K. Kamaraju, M.-S. Chiu, *Org. Process Res. Dev.* **2015**, *19 (1)*, 3–62. DOI: 10.1021/op500261y

[22] Z. K. Nagy, G. Fevotte, H. Kramer, L. L. Simon, *Chem. Eng. Res. Des.* **2013**, *91 (10)*, 1903–1922. DOI: 10.1016/j.cherd.2013.07.018

[23] M. Kempkes, T. Vetter, M. Mazzotti, *Chem. Eng. Sci.* **2010**, *65 (4)*, 1362–1373. DOI: 10.1016/j.ces.2009.10.008

[24] D. L. T. Nguyen, K.-J. Kim, *Chem. Eng. Technol.* **2015**, *38 (6)*, 1059–1067. DOI: 10.1002/ceat.201400725

[25] R. M. Carter, Y. Yan, P. Lee, *IEEE Trans. Instrum. Meas.* **2006**, *55 (6)*, 2034–2038. DOI: 10.1109/Tim.2006.887039

[26] C. Tachtatzis, R. Sheridan, C. Michie, R. C. Atkinson, A. Cleary, J. Dziewierz, I. Andonovic, N. E. B. Briggs, A. J. Florence, J. Sefcik, *Chem. Eng. Sci.* **2015**, *133*, 82–90. DOI: 10.1016/j.ces.2015.01.038

[27] E. Darakis, T. Khanam, A. Rajendran, V. Kariwala, T. J. Naughton, A. K. Asundi, *Chem. Eng. Sci.* **2010**, *65 (2)*, 1037–1044. DOI: 10.1016/j.ces.2009.09.057

[28] M. Jiang, C. D. Papageorgiou, J. Waetzig, A. Hardy, M. Langston, R. D. Braatz, *Cryst. Growth Des.* **2015**, *15 (5)*, 2486–2492. DOI: 10.1021/acs.cgd.5b00263

[29] M. N. Gulari, A. Tripathi, M. Ghannad-Rezaie, N. Chronis, *Micromachines* **2014**, *5 (3)*, 607–621. DOI: 10.3390/mi5030607

